Modeling Temperature-Dependent Avalanche Characteristics of InP

Jonathan D. Petticrew, *Student Member, IEEE*, Simon J. Dimler, *Member, IEEE, Member, OSA*, Chee Hing Tan, *Senior Member, IEEE*, and Jo Shien Ng, *Member, IEEE*

***Abstract*—Avalanche photodiodes (APDs), and single photon avalanche diodes (SPADs), with InP avalanche regions and InGaAs absorption regions, are used for detecting weak infrared light at ∼1.55 μm wavelength. These devices are often cooled to below room temperature during operation yet both validated simulation models and impact ionization coefficients that accurately describe the avalanche characteristics of InP are lacking in the temperature range of interest (200 K to room temperature). In this article we present an accessible, validated temperature dependent simulation model for InP APDs/SPADs. The model is capable of simulating avalanche gain, excess noise, breakdown voltage, and impulse current at 150–300 K. Temperature dependent ionization coefficients in InP, which may be used with other APD/SPAD simulation models, are also presented. The data reported in this article is available from the ORDA digital repository (DOI: 10.15131/shef.data.c.4373006).**

***Index Terms*—Avalanche breakdown, avalanche photodiodes, impact ionization, indium phosphide.**

I. Introduction

LIGHT detection and ranging (LiDAR) systems [1] for long-range three-dimensional imaging are increasingly important in applications such as autonomous vehicles, surveillance, remote sensing, and gas detection. The majority of LiDAR systems use a silicon Avalanche Photodiode (APD) or a silicon Single Photon Avalanche Diode (SPAD) to detect the weak optical signals. The operation wavelength for these Si detectors is up to ∼1 μm, which has several drawbacks for long-range LiDAR since optical signals at these wavelengths are attenuated heavily by atmospheric obscurants (e.g., smoke, dust, and water vapor), and are not eye-safe. The level of signal attenuation may be significantly reduced by increasing the operating wavelength to 1.55 μm and optical signals at 1.55 μm can also have a $\sim 10^5$ times greater energy c.f. 633 nm whilst still remaining eye-safe (assuming 1 ns - 10 μs pulse duration) [2]. To detect 1.55 μm wavelength optical signals, the Si detector must be replaced by an appropriate alternative, such as $In_{0.53}Ga_{0.47}As$/InP APD or SPAD. In LiDAR applications, $In_{0.53}Ga_{0.47}As$/InP APDs or SPADs are often cooled to below room temperature (e.g., 200–240 K, [3], [4]) to reduce reverse leakage currents or dark counts respectively, to improve signal-to-noise performance. In addition to LiDAR systems, $In_{0.53}Ga_{0.47}As$/InP SPADs are used in receiver modules of Quantum Key Distribution (QKD) systems [5] and they are similarly cooled during operation.

In $In_{0.53}Ga_{0.47}As$/InP APDs and SPADs, many of the important characteristics are determined by the impact ionization process taking place in the devices' InP avalanche region. Since $In_{0.53}Ga_{0.47}As$/InP APDs and SPADs are cooled in operation, accurate simulation models for the impact ionization process at 200 K to room temperature capable of simulating carrier distribution, and scattering processes, will assist the optimization of $In_{0.53}Ga_{0.47}As$/InP APDs and SPADs.

Impact ionization of InP at room temperature has been extensively studied experimentally [6]–[8], with characteristics of avalanche gain versus bias, $M(V)$, and excess noise factor versus gain, $F(M)$, reported from multiple diode structures [7], [8]. Hence room temperature field dependent ionization coefficients for electrons, $\alpha(\zeta)$, and holes, $\beta(\zeta)$, along with ionization threshold energies, have been extracted [8], [9], and they can be used in accessible simulation models such as those based on recurrence equations [9], Random Path Lengths [10], drift-diffusion [11], and analytical methods [12].

Data from InP impact ionization at low temperatures is more limited. Reported work, [13]–[15], has relied on diffused junctions to create their InP diodes, so are likely to suffer from significant uncertainties in the electric field values. Crucially, ionization coefficients were not presented in [13]. Independent efforts to extract the ionization coefficients from their presented experimental results would be difficult due to incomplete knowledge of the doping profiles of the measured diodes. Temperature dependent ionization coefficients for InP were reported in [14]. However, their values for room temperature are significantly lower than other reports [6]–[8], probably due to further uncertainties arising from using only a single InP diode structure and incorrect experimental values of avalanche gain data (avalanche gain values from mixed carrier injection were assumed as values from pure hole injection in [14]).

Several simulation models have been reported for temperature dependence of breakdown voltage of $In_{0.53}Ga_{0.47}As$/InP APDs [12], [16]–[18], but most did not present rigorous validation. All, except [18], were validated against only a single

Manuscript received July 24, 2019; accepted October 7, 2019. Date of publication October 17, 2019; date of current version February 12, 2020. This work was supported by the Engineering and Physical Sciences Research Council under Grant EP/M506618/1. *(Corresponding author: Jo Shien Ng.)*

The authors are with the Department of Electronic and Electrical Engineering, University of Sheffield, Sheffield S3 7HQ, U.K. (e-mail: jdpetticrew1@sheffield.ac.uk; s.dimler@sheffield.ac.uk; c.h.tan@sheffield.ac.uk; j.s.ng@sheffield.ac.uk).

This article has supplementary downloadable material available at http://ieeexplore.ieee.org, provided by the authors.

Digital Object Identifier 10.1109/JLT.2019.2948072

This work is licensed under a Creative Commons Attribution 4.0 License. For more information, see http://creativecommons.org/licenses/by/4.0/

$In_{0.53}Ga_{0.47}As$/InP APD design. A Simple Monte Carlo (SMC) model for the impact ionization process, first reported in 1999 [19], has recently been made available [20], with parameter files published for a range of avalanche materials including Si [21]. The SMC model is far less computationally intensive compared to Analytical and Full Band Monte Carlo models [22], [23], whilst incorporating sufficient impact ionization statistics (including dead space effects) to simulate a wide range of APD/SPAD designs, e.g., with thin avalanche regions and/or rapidly varying electric field profiles.

In this paper we present an SMC parameter set for InP at 150 to 300 K, for use with our SMC simulator [20]. We comprehensively validated against a range of experimental data, including material characteristics such as saturation velocities, impact ionization coefficients for electrons and holes (α and β), as well as device characteristics such as *M*(*V*) and *F*(*M*) from multiple APD structures. In addition, we present temperature dependent impact ionization coefficients of InP that can be used with other models requiring ionization coefficients as inputs.

II. Model

The SMC model has been extensively described in previous publications [19], [21] so only a brief description will be included here with an emphasis on the temperature dependence [24]. In the SMC model, a free carrier drifts in the depletion region for a random distance before undergoing one of three mechanisms: intervalley phonon absorption; intervalley phonon emission; or impact ionization. After the free carrier has undergone one of these mechanisms, a new random scattering direction is chosen to update the momentum of the carrier. The intervalley phonon emission and intervalley phonon absorption rates, R_{em} and R_{ab}, are

$$R_{em}(T) = \frac{N(T)+1}{\lambda(T)\ (2N(T)\ +1)}\sqrt{\frac{2\,(E-\hbar\omega)}{m^*}}$$

and

$$R_{ab}(T) = \frac{N(T)}{\lambda(T)\ (2N(T)\ +1)}\sqrt{\frac{2\,(E+\hbar\omega)}{m^*}},$$

where *T* is the temperature, *N*(*T*) is the temperature dependent phonon occupation factor, $\lambda(T)$ is the temperature dependent mean free path between scattering events, *E* is the energy of the carrier, $\hbar\omega$ is the mean phonon energy, and m^* is the effective mass of the carrier. *N*(*T*) is given by

$$N\,(T) = \left(\exp\left(\frac{\hbar\omega}{kT}\right) - 1\right)^{-1},$$

where k is Boltzmann's constant. Since $\lambda \sim (1+2N)^{-1}$ the temperature dependent mean free path takes the form of

$$\lambda\,(T) = \lambda\,(300\,K) \times \frac{2N\,(300\,K)+1}{2N\,(T)+1},$$

where *N*(300 K) and λ(300 K) are the phonon occupation factor and mean free path respectively at 300 K. Within this model, temperature dependence is described by *N*(*T*) and λ(*T*). The other SMC parameters are either known to change very slowly with temperature or are assumed to be temperature independent. The rate of impact ionization, R_{ii}, is calculated using the Keldysh equation [25],

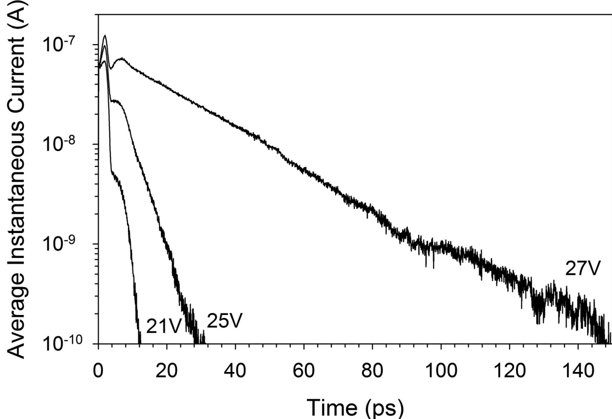

Fig. 1. Average Impulse currents for the 21, 25, and 27 V operation of device C with corresponding gain values of 1.26, 2.67, and 12.53.

$$R_{ii} = C_{ii}\left(\frac{E-E_{th}}{E_{th}}\right)^{\gamma},$$

where γ is the softness factor of impact ionization, C_{ii} is the prefactor of impact ionization rate, and E_{th} is the threshold energy of impact ionization. Ramo's theorem [26] is used to calculate the instantaneous current from the movement of the carriers within the device, which make up the impulse current. Avalanche gain from the injection of a single carrier (electron or hole) is given by the area under the impulse current versus time characteristics. The impulse current versus time data can also be used to calculate theoretical response times and bandwidths. Examples of average impulse current characteristics from the model are shown in Fig. 1. The impact ionization coefficient for a given electric field, is determined by the inverse of the mean distance travelled between 20000 consecutive impact ionization events. When simulating a given device design, the electric field profile at a given reverse bias was calculated using a 1D Poisson field solver.

III. Model Validation

A value of 42 meV was used for $\hbar\omega$, based on the longitudinal optical phonon frequency of 345 cm^{-1} in InP [27]. The effective masses of the carriers were adjusted so that the saturation velocities at 300 K produced by the SMC model matched the reported values of 6.8 × 10^6 and 7.0 × 10^6 cm.s^{-1} for electrons and holes respectively [28], [29], as shown in Fig. 2(a). Values of C_{ii} and λ(300 K) were adjusted so that the model produces $\alpha(\zeta)$ and $\beta(\zeta)$ in line with [6]–[8], as shown in Fig. 2(b).

Further adjustments to C_{ii} and λ(300 K) values relied on comparisons between simulated and reported *M*(*V*) and *F*(*M*) characteristics for six InP APDs at 300 K [8]. These are devices A–F, whose structural details are summarized in Table I. The doping information was deduced from fitting room temperature capacitance-voltage data of the devices (multiple different-sized

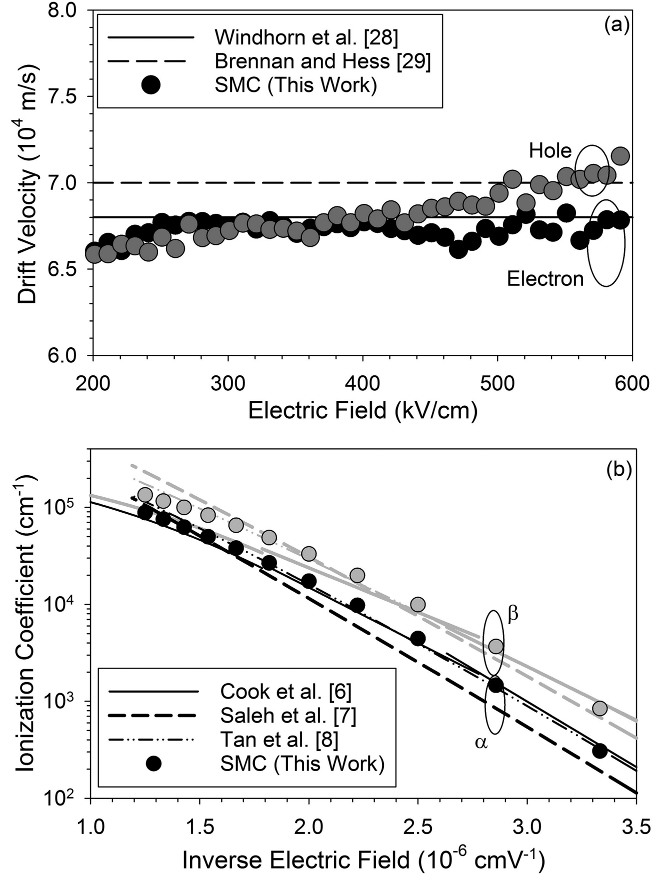

Fig. 2. Comparisons of (a) drift velocities and (b) impact ionization coefficients at room temperature of the InP SMC model (symbols) with reference data (lines), which are taken from [28,29] for (a) and [6,7,8] for (b).

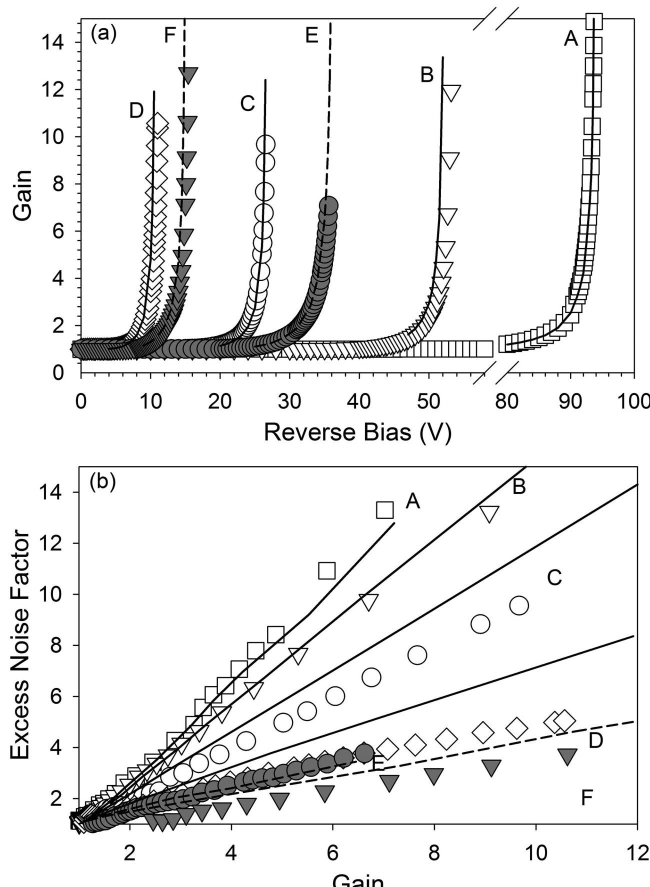

Fig. 3. Comparison of (a) M(V) and (b) F(M) characteristics simulated by the SMC model (lines) with data from [8] (symbols), for four InP P-I-N (device A-D) and two InP N-I-P devices (device E and F) at room temperature.

TABLE I
STRUCTURE DETAILS OF DEVICES USED IN MODEL VALIDATION AT ROOM TEMPERATURE (A-F) AND LOW TEMPERATURES (C-G)

Device	Intrinsic Region Width (μm)	Structure	P/N doping (10^{18} cm^{-3})	I doping (10^{15} cm^{-3})
A [8]	2.5	P-I-N	0.6	0.3
B [8]	1.25	P-I-N	0.7	2
C [8]	0.545	P-I-N	1.1	1
D [8]	0.125	P-I-N	1.3	10
E [8]	0.8	N-I-P	0.8	0.8
F [8]	0.23	N-I-P	0.9	4
G [18]	1.63	P-I-N	1.8	1

TABLE II
INP SMC MODEL PARAMETERS USED IN THIS WORK

	Electrons	Holes
Prefactor of impact ionization rate, C_{ii} (s^{-1})	3.5×10^{12}	8.5×10^{12}
Threshold Energy, E_{th} (eV)	1.55	1.55
Softness Factor, γ	0.7	0.7
Phonon Energy, $\hbar\omega$ (meV)	42	
Mean free path at 300K, $\lambda(300K)$ (Å)	41	42
Effective mass, m^* (kg)	$0.62m_0$	$0.63m_0$
Relative Permittivity	12.5	

diodes for each device). The unintentional doping in all structures, except device E, is n-type. The simulated $M(V)$ and $F(M)$ characteristics are in good agreement with data from [8], as shown in Fig. 3(a) and (b). The resultant InP SMC model parameter set is summarized in Table II.

Validation of the InP SMC model at lower temperatures consisted of simulations of $M(V)$ characteristics of devices C-G at 290, 250, 200, 150, 100, and 77 K. These simulations are compared to data from [18] in Fig. 4. Simulated and experimental data for all devices are in agreement for temperatures from 290 K down to 150 K. As temperature decreases below 150 K, there is growing discrepancy between the simulations and experimental data, particularly for the devices with wider avalanche regions. Hence the model is deemed to be valid from 290 K to 150 K. The discrepancy observed for comparisons at 100 and 77 K could be caused by insufficient knowledge of doping profiles for temperatures <150 K where there is a lower level of dopant activation.

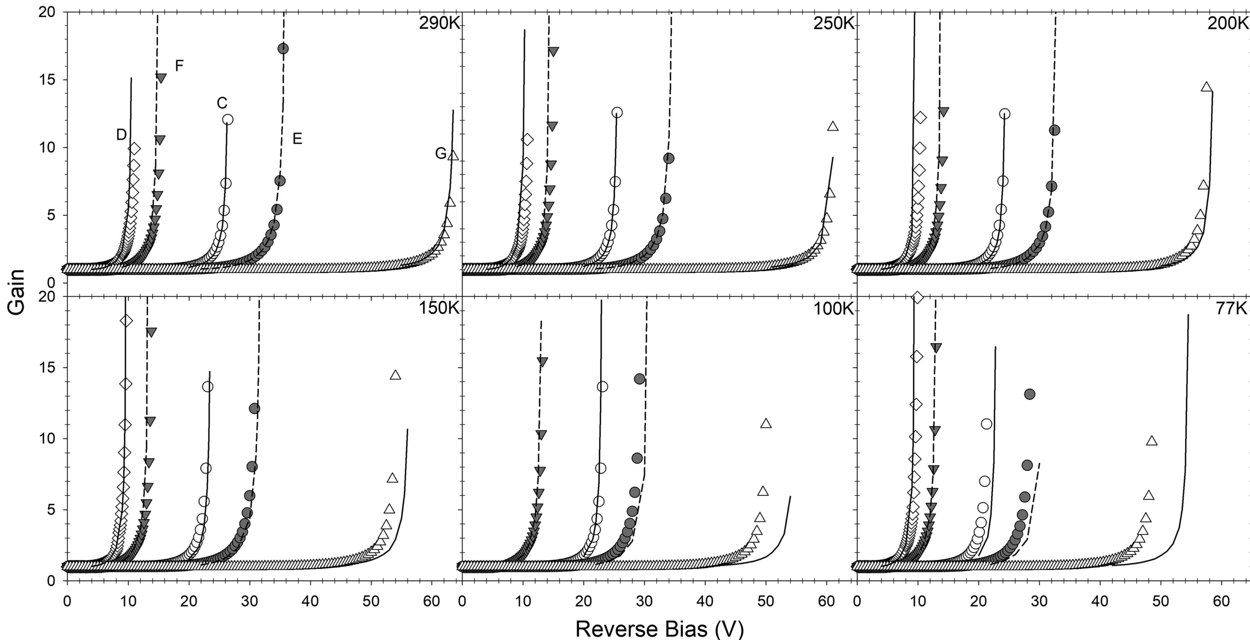

Fig. 4. Comparison of M(V) simulated by the SMC model (lines) with experimental results (symbols) [18], for three InP P-I-N (device C, D, and G) and two N-I-P devices (device E and F) at 290, 250, 200, 150, 100, and 77 K. Device D was not measured at 100 K.

IV. Ionization Coefficients

From the impact ionization simulations it is possible to generate ionization path length probability density functions (PDFs) for each simulated electric field strength. As part of this work probability density functions for 400–800 kV.cm^{-1} have been generated in 50 kV.cm^{-1} steps for electrons and holes at 150, 200, 250, and 290 K. Fitting these ionization path length PDFs, $h_e(x)$ for electrons and $h_h(x)$ for holes, using the form,

$$h_e(x) = \begin{cases} 0, & x \le d_e \\ \alpha^* \exp(-\alpha^* \ (x - d_e)), & x > d_e \end{cases}$$

and

$$h_h(x) = \begin{cases} 0, & x \le d_h \\ \beta^* \exp(-\beta^* \ (x - d_h)), & x > d_h \end{cases}$$

where d_e and d_h are the electron and hole deadspaces respectively (where deadspace is defined as the minimum distance an electron or hole can travel before it can undergo impact ionization) and *x* is the carrier path length. Fitting the ionization path length PDFs to $h_e(x)$ and $h_h(x)$ allowed us to extract $\alpha^*(E)$ and $\beta^*(E)$ in the form

$$\alpha^*(E) \ and \ \beta^*(E) = A_f \times \exp\left[-\left(\frac{B_f}{E}\right)^{C_f}\right],$$

for each temperature, with values of fitting parameters A_f, B_f, C_f summarized in Table III.

Using the provided expressions for $\alpha^*(E)$ and $\beta^*(E)$ with threshold energies of 2.8 eV for electrons and 3.0 eV for holes [8], allowed for the temperature dependent gain simulation of devices C-G using the recurrence equations [30], as shown in

TABLE III
Electric Field Dependence of α^* and β^* at 150 to 290 K, Using the Expression $\alpha^*(E)$ *or* $\beta^*(E) = A_f \times \exp[-(\frac{B_f}{E})^{C_f}]$

Temperature (K)		A_f ($10^6 \times$ cm^{-1})	B_f ($10^6 \times$ cm^{-1})	C_f
290	α^*	2.55×10^2	2.15×10^2	1.08
	β^*	9.80×10^1	1.00×10^2	1.60
250	α^*	4.70×10^2	2.96×10^2	0.94
	β^*	$1.4.3 \times 10^2$	1.14×10^2	1.48
200	α^*	1.70×10^2	1.60×10^2	1.21
	β^*	6.3×10^2	2.74×10^2	0.90
150	α^*	4.03×10^2	7.73×10^1	0.44
	β^*	1.68	1.15	1.39

Figs. S1-4. A comparison of room temperature *F*(*M*) is also presented in Fig. S5.

V. Conclusion

We have presented a simulation model for temperature dependent InP avalanche characteristics for 150–300 K. This model has been validated against experimental results of avalanche gain and excess noise factor from InP APDs at 300 K, with avalanche widths from 0.125–2.5 μm, along with experimental avalanche gain results for InP APDs at temperatures from 150–300 K and with avalanche widths of 0.125–1.63 μm. This validated model has subsequently been used to calculate the temperature dependent impact ionization coefficients of InP between 150–290 K.

References

[1] A. M. Pawlikowska, A. Halimi, R. A. Lamb, and G. S. Buller, "Single-photon three-dimensional imaging at up to 10 kilometers range," *Opt. Express*, vol. 25, no. 10, pp. 11919–11931, May 2017.

[2] *Safety of Laser Products. Part 1: Equipment Classification and Requirements*, British Standards Institute, BS EN 60825-1, 2014.

[3] F. Acerbi, M. Anti, A. Tosi, and F. Zappa, "Design criteria for InGaAs/InP single-photon avalanche diode," *IEEE Photon. J.*, vol. 5, no. 2, Apr. 2013, Art. no. 6800209.
[4] L. C. Comandar *et al.*, "Gigahertz-gated InGaAs/InP single-photon detector with detection efficiency exceeding 55% at 1550 nm," *J. Appl. Phys.*, vol. 117, no. 8, Feb. 2015, Art. no. 083109.
[5] A. Aguado *et al.*, "Secure NFV orchestration over an SDN-controlled optical network with time-shared quantum key distribution resources," *IEEE J. Lightw. Technol.*, vol. 35, no. 8, pp. 1357–1362, Apr. 2017.
[6] L. W. Cook, G. E. Bulman, and G. E. Stillman, "Electron and hole impact ionization coefficients in InP determined by photomultiplication measurements," *Appl. Phys. Lett.*, vol. 40, no. 7, pp. 589–591, Apr. 1982.
[7] M. A. Saleh *et al.*, "Impact-ionization and noise characteristics of thin III-V avalanche photodiodes," *IEEE Trans. Electron Devices*, vol. 48, no. 12, pp. 2722–2731, Dec. 2001.
[8] L. J. J. Tan, J. S. Ng, C. H. Tan, and J. P. R. David, "Avalanche noise characteristics in submicron InP diodes," *IEEE J. Quantum Electron.*, vol. 44, no. 4, pp. 378–382, Apr. 2008.
[9] J. S. Ng, C. H. Tan, G. J. Rees, and J. P. R. David, "Effects of dead space on breakdown probability in Geiger mode avalanche photodiode," *J. Mod. Opt.*, vol. 54, no. 2/3, pp. 353–360, Jan. 2007.
[10] S. C. Liew Tat Mun *et al.*, "A theoretical comparison of the breakdown behavior of $In_{0.52}Al_{0.48}As$ and InP near-infrared single-photon avalanche photodiodes," *IEEE J. Quantum Electron.*, vol. 45, no. 5, pp. 566–571, May 2009.
[11] N. R. Das and M. Jamal Deen, "Low-bias performance of avalanche photodetector. A time-domain approach," *IEEE J. Quantum Electron.*, vol. 37, no. 1, pp. 69–74, Jan. 2001.
[12] C. L. F. Ma, M. J. Deen, L. E. Tarof, and J. C. H. Yu, "Temperature dependence of breakdown voltages in separate absorption, grading, charge, and multiplication InP/InGaAs avalanche photodiodes," *IEEE Trans. Electron Devices*, vol. 42, no. 5, pp. 810–818, May 1995.
[13] Y. Takanashi and Y. Horikoshi, "Temperature dependence of ionization coefficients for InP and 1.3 μm InGaAsP avalanche photodiodes," *Jpn. J. Appl. Phys.*, vol. 20, no. 10, pp. 1907–1913, Oct. 1981.
[14] F. Osaka, T. Mikawa, and T. Kaneda, "Low-temperature characteristics of electron and hole ionization coefficients in (100) oriented $Ga_{1-x}In_x As_yP_{1-y}$," *Appl. Phys. Lett.*, vol. 46, no. 12, pp. 1138–1140, Jun. 1985.
[15] C. H. Tan *et al.*, "Improved excess noise and temperature dependence of multiplication characteristics in thin InP avalanching regions," in *Proc. Conf. Indium Phosph.*, Davos, Switzerland, 1999, pp. 295–298.
[16] Y. Zhao *et al.*, "Temperature dependence simulation and characterization for InP/InGaAs avalanche photodiodes," *Frontiers Optoelectron.*, Jan. 2019.
[17] K. Taguchi, T. Torikai, Y. Sugimoto, K. Makita, and H. Ishihara, "Temperature dependence of impact ionization coefficients in InP," *J. Appl. Phys.*, vol. 59, no. 2, pp. 476–481, Jan. 1986.
[18] L. J. J. Tan *et al.*, "Temperature dependence of avalanche breakdown in InP and InAlAs," *IEEE J. Quantum Electron.*, vol. 46, no. 8, pp. 1153–1157, Aug. 2010.
[19] S. A. Plimmer, J. P. R. David, D. S. Ong, and K. F. Li, "A simple model for avalanche multiplication including deadspace effects," *IEEE Trans. Electron Devices*, vol. 46, no. 4, pp. 769–775, Apr. 1999.
[20] J. D. Petticrew, S. J. Dimler, and J. S. Ng, "Simple Monte Carlo simulator for modelling linear mode and geiger mode avalanche photodiodes in C++," *J. Open Res. Softw.*, vol. 6, p. 17, May 2018.
[21] J. D. Petticrew, S. J. Dimler, X. Zhou, A. P. Morrison, C. H. Tan, and J. S. Ng, "Avalanche breakdown timing statistics for silicon single photon avalanche diodes," *IEEE J. Sel. Topics Quantum Electron.*, vol. 24, no. 2, Mar./Apr. 2018, Art no. 3801506.
[22] S. Zhang and Y. Zhao, "Study on impact ionization in charge layer of InP/InGaAs SAGCM avalanche photodiodes," *Opt. Quantum Electron.*, vol. 47, no. 8, pp. 2689–2696, Aug. 2015.
[23] D. Dolgos, H. Meier, A. Schenk, and B. Witzigmann, "Full-band Monte Carlo simulation of high-energy carrier transport in single photon avalanche diodes with multiplication layers made of InP, InAlAs, and GaAs," *J. Appl. Phys.*, vol. 111, no. 10, p. 104508, May 2012.
[24] C. Groves, C. N. Harrison, J. P. R. David, and G. J. Rees, "Temperature dependence of breakdown voltage in $Al_xGa_{1-x}As$," *J. Appl. Phys.*, vol. 96, no. 9, pp. 5017–5019, Nov. 2004.
[25] L. V. Keldysh, "Kinetic theory of impact ionization in semiconductors", *Sov. Phys. JETP*, vol. 37, no. 3, pp. 509–518, Mar. 1959.
[26] S. Ramo, "Currents induced by electron motion," *Proc. IRE*, vol. 27, no. 9, pp. 584–585, Sep. 1939.
[27] D. J. Lockwood, G. Yu, and N. L. Rowell, "Optical phonon frequencies and damping in AlAs, GaP, GaAs, InP, InAs, and InSb studied by oblique incidence infrared spectroscopy," *Solid State Commun.*, vol. 136, no. 7, pp. 404–409, Nov. 2005.
[28] T. H. Windhorn, L. W. Cook, M. A. Haase, and G. E. Stillman, "Electron transport in InP at high electric fields," *Appl. Phys. Lett.*, vol. 42, no. 8, pp. 725–727, Apr. 1983.
[29] K. Brennan and K. Hess, "Theory of high-field transport of holes in GaAs and InP," *Phys. Rev. B*, vol. 29, no. 10, pp. 5581–5590, 1984.
[30] M. M. Hayat, B. E. A. Saleh, and M. C. Teich, "Effect of dead space on gain and noise of double-carrier-multiplication avalanche photodiodes," *IEEE Trans. Electron Devices*, vol. 39, no. 3, pp. 546–552, Mar. 1992.

Jonathan D. Petticrew (S'16) received the M.Phys. degree in physics, in 2015, from the University of Sheffield, Sheffield, U.K., where he is currently working toward the Ph.D. degree in the design and fabrication of single photon detectors.

Simon J. Dimler received the M.Eng. and Ph.D. degrees in electronic and electrical engineering from the University of Sheffield, Sheffield, U.K. His current research is focused on the development of single photon detectors and instrumentation for the characterization of photodetectors. He is a Member of the Optical Society.

Chee Hing Tan (M'95–SM'17) received the B.Eng. and Ph.D. degrees in electronic engineering from the Department of Electronic and Electrical Engineering, University of Sheffield, Sheffield, U.K., in 1998 and 2002, respectively.

He is currently a Professor of Opto-Electronic Sensors with the Department of Electronic and Electrical Engineering, University of Sheffield. He has extensive experience in the characterization and modeling of high-speed low-noise avalanche photodiodes and phototransistors. His current research interests include single-photon avalanche diodes, mid-infrared photodiodes, quantum-dot infrared detectors, X-ray detectors, ultrahigh-speed avalanche photodiodes, and phototransistors.

Jo Shien Ng (M'99) received the B.Eng. and Ph.D. degrees in electronic engineering from the University of Sheffield, Sheffield, U.K., in 1999 and 2003, respectively.

She is currently a Professor of Semiconductor Devices with the Department of Electronic and Electrical Engineering, University of Sheffield. She was a Royal Society Research Fellow with the same department between 2006 and 2016. Her research interests include avalanche photodiodes, Geiger-mode avalanche photodiodes, and material characterization.